

# SDPose: EXPLOITING DIFFUSION PRIORS FOR OUT-OF-DOMAIN AND ROBUST POSE ESTIMATION

Shuang Liang<sup>1,4\*</sup> Jing He<sup>3</sup> Chuanmeizhi Wang<sup>1</sup> Lejun Liao<sup>2</sup> Guo Zhang<sup>1</sup>  
 Yingcong Chen<sup>3,5</sup> Yuan Yuan<sup>2✉</sup>

<sup>1</sup>Rama Alpaca Technology Company <sup>2</sup>Boston College <sup>3</sup>HKUST(GZ)  
<sup>4</sup>The University of Hong Kong <sup>5</sup>HKUST

Project page: <https://t-s-liang.github.io/SDPose>



Figure 1: **SDPose: OOD-robust pose via diffusion priors.** On stylized paintings, SDPose surpasses Sapiens and ViTPose++-H, matching SoTA on COCO and setting new records on HumanArt and COCO-OOD; yellow boxes show baseline failures.

\*Work done during an internship at Rama Alpaca Technology.

## ABSTRACT

Pre-trained diffusion models provide rich multi-scale latent features and are emerging as powerful vision backbones. While recent works such as Marigold (Ke et al., 2024) and Lotus (He et al., 2024) adapt diffusion priors for dense prediction with strong cross-domain generalization, their potential for structured outputs (e.g., human pose estimation) remains under-explored. In this paper, we propose **SDPose**, a fine-tuning framework built upon Stable Diffusion to fully exploit pre-trained diffusion priors for human pose estimation. First, rather than modifying cross-attention modules or introducing learnable embeddings, we directly predict keypoint heatmaps in the SD U-Net’s image latent space to preserve the original generative priors. Second, we map these latent features into keypoint heatmaps through a lightweight convolutional pose head, which avoids disrupting the pre-trained backbone. Finally, to prevent overfitting and enhance out-of-distribution robustness, we incorporate an auxiliary RGB reconstruction branch that preserves domain-transferable generative semantics. To evaluate robustness under domain shift, we further construct **COCO-OOD**, a style-transferred variant of COCO with preserved annotations. With just one-fifth of the training schedule used by Sapiens on COCO, SDPose attains parity with Sapiens-1B/2B on the COCO validation set and establishes a new state of the art on the cross-domain benchmarks HumanArt and COCO-OOD. Furthermore, we showcase SDPose as a zero-shot pose annotator for downstream controllable generation tasks, including ControlNet-based image synthesis and video generation, where it delivers qualitatively superior pose guidance.

## 1 INTRODUCTION

With the recent rise of embodied AI, video generation, and 3D asset rendering, the need for cross-domain-robust human pose estimation has become critical in robotics as well as in film, animation, and game production. Although recent advances on academic benchmarks such as MS COCO (Lin et al., 2014) using models such as DWPose (Yang et al., 2023), RTMPose (Jiang et al., 2023) and OpenPose (Martinez, 2019), as well as approaches leveraging large pretrained backbones such as ViTPose (Xu et al., 2022; 2023) and Sapiens (Khirodkar et al., 2024), have achieved strong in-domain accuracy, they often exhibit severe performance degradation under domain shifts and require substantial fine-tuning efforts.

Recently, pre-trained diffusion models such as Stable Diffusion (Rombach et al., 2022) have emerged as robust vision backbones. A growing body of work has shown that with fine-tuning and adaptation, diffusion priors can be repurposed for 3D generation (Cheng et al., 2023; Lin et al., 2025; Long et al., 2024), segmentation (Karmann & Urfalioglu, 2025), and dense prediction tasks (Ke et al., 2024; He et al., 2024), while consistently demonstrating strong cross-domain robustness and highlighting their potential for leveraging intra-visual multimodality in generative priors. However, their potential for structured and semantically aware outputs, particularly in human pose estimation, remains largely unexplored. Concurrent efforts like GenLoc (Wang et al., 2025a) and Diff-Tracker (Zhang et al., 2024) indicate that generative priors can benefit keypoint localization and tracking by steering learnable condition embeddings and adapting the diffusion model’s cross-attention. We instead examine a complementary axis: can one rely purely on SD U-Net latent features, without attention read-outs or condition tokens, to produce reliable pose heatmaps?

To bridge this gap and systematically study how to leverage the rich latent features for robust, cross-domain pose estimation, we propose **SDPose**, a fine-tuning framework with three key components: **(i) Latent-space preservation.** We operate entirely in the SD U-Net’s image latent space without modifying cross-attention modules or adding learnable embeddings, thus preserving pretrained visual semantics and feature geometry. **(ii) Lightweight pose decoder head.** We employ one deconvolution layer (kernel size 4) followed by two  $1 \times 1$  convolutions to map intermediate U-Net features directly into keypoint heatmaps,

minimizing disruption to the pretrained backbone. **(iii) RGB reconstruction regularization.** We add an auxiliary reconstruction branch that regularizes fine-tuning, helping to maintain domain-transferable generative semantics and improve out-of-distribution robustness. Furthermore, to systematically evaluate robustness under domain shift, we introduce **COCO-OOD**, a style-transferred extension of COCO annotations featuring oil painting domains, which bridges the gap in benchmarking for generalization robustness evaluation.

On COCO (Lin et al., 2014) and COCO-WholeBody (Jin et al., 2020), SDPose delivers in-domain performance on par with the current SoTA, Sapiens (Khirodkar et al., 2024). Under domain shift (HumanArt (Ju et al., 2023), COCO-OOD), it sets a new state of the art while using only one-fifth of Sapiens’s fine-tuning epochs, highlighting the efficiency and cross-domain robustness of generative priors. Beyond quantitative benchmarks, we further demonstrate SDPose as a zero-shot pose annotator for downstream controllable generation tasks, including ControlNet-based image synthesis and video generation, where it provides reliable and qualitatively superior pose guidance.

## 2 RELATED WORKS

### 2.1 LATENT DIFFUSION MODELS

Latent diffusion models (LDMs), built on DDPM and further advanced by ODE and SDE samplers (Ho et al., 2020; Song et al., 2020b;a; Lu et al., 2022; Rombach et al., 2022), have gained traction over the past few years. Classic architectures, such as the UNet-based Stable Diffusion and Diffusion Transformers (DiT) (Peebles & Xie, 2023; Esser et al., 2024), have demonstrated strong performance across diverse conditional generation tasks (Zhang et al., 2023). Pretrained on large-scale datasets such as LAION-5B (Schuhmann et al., 2022), generative models like Stable Diffusion provide rich visual priors that can be effectively leveraged for a wide range of tasks. Recent advances in flow-matching (Lipman et al., 2022; Esser et al., 2024; Xie et al., 2024) further show that latent diffusion models can achieve high-quality synthesis with only a few sampling steps. These developments highlight the power of latent generative priors as a strong visual foundation.

### 2.2 LEVERAGING DIFFUSION PRIORS FOR PREDICTION TASKS

A growing body of work has explored repurposing pretrained latent diffusion priors for dense prediction tasks. Marigold (Ke et al., 2024) adapts Stable Diffusion by fine-tuning only the denoising U-Net using synthetic data, delivering high-quality depth results. Later, subsequent methods such as Lotus (He et al., 2024) and GenPercept (Xu et al., 2024) both adopt a deterministic one-step fine-tuning strategy, removing the multi-step stochastic diffusion process and directly predicting task annotations, which significantly improves both accuracy and inference speed. In contrast, leveraging latent diffusion priors for structured outputs (e.g., human pose) remains underexplored. Prior works such as GenLoc (Wang et al., 2025a) and Diff-Tracker (Zhang et al., 2024) freeze Stable Diffusion backbone and use learnable condition or prompt embeddings to read cross-attention maps, rather than decoding from U-Net latent features, aiming at zero-/few-shot and schema-flexible generalization. We instead remain in the image latent space, treat the SD U-Net as a multi-scale backbone, and attach a minimal convolutional head to produce keypoint heatmaps, retaining SD-native visual semantics and improves robustness under domain shift.

### 2.3 HUMAN POSE ESTIMATION

Human pose estimation is a classic and fundamental task in computer vision. Early approaches predominantly relied on CNN backbones such as HRNet (Sun et al., 2020) and CSPNeXt (Chen et al., 2024), coupled with heuristically designed decoding heads. Models like RTMPose (Jiang et al., 2023) and DWPose (Yang et al., 2023) achieved strong performance on academic benchmarks such as COCO and COCO WholeBody. However, these models exhibit limited generalization when transferring from real human figures to out-of-domain cases, such as anime characters. More recently, fine-tuned methods built on extensive pre-trained vision backbones, such as ViTPose (Xu et al., 2022; 2023) and

Sapiens (Khirodkar et al., 2024), have achieved SoTA results on standard benchmarks, demonstrating the benefit of leveraging pre-trained foundation models for pose estimation. Nevertheless, these methods incur high fine-tuning costs, as they require large task-specific datasets and lengthy training schedules to achieve competitive performance. In this paper, we demonstrate that fine-tuning the Stable Diffusion pipeline with minimal architectural modifications can address both the generalization gap and the high fine-tuning cost.

### 3 PRELIMINARIES

#### 3.1 HEATMAP REPRESENTATION AND UNBIASED DATA PROCESSING (UDP)

Let  $(x_i, y_i)$  denote the  $i$ -th ground-truth keypoint in an  $H \times W$  image. The standard heatmap representation encodes each keypoint as

$$H_i(u, v) = \exp\left(-\frac{(u - x_i)^2 + (v - y_i)^2}{2\sigma^2}\right), \quad (\hat{x}_i, \hat{y}_i) = \arg \max_{u, v} H_i(u, v).$$

While widely adopted, this discrete pixel-space formulation suffers from quantization bias: predicted coordinates become misaligned under flips, scales, or rotations since the argmax operation only yields integer positions. To address this issue, we adopt the Unbiased Data Processing (UDP) method (Huang et al., 2020), which removes quantization bias by estimating keypoints in a continuous domain. Following common practice, the heatmap is generated at one-quarter resolution of the input image, which balances localization accuracy with computational efficiency.

#### 3.2 PARAMETERIZATION FOR LATENT DIFFUSION MODEL

Traditional latent diffusion models (LDMs) (Ho et al., 2020) adopt the  $\epsilon$ -prediction parameterization, where the denoiser  $f_\theta$  is trained to predict the Gaussian noise  $\epsilon_t$  added at timestep  $t$ :

$$\hat{\epsilon}_t = f_\theta(z_t, t),$$

with  $z_t$  denoting the noisy latent at step  $t$ . The clean latent  $x_0$  can then be recovered by

$$\hat{x}_0 = \frac{z_t - \sqrt{1 - \alpha_t} \hat{\epsilon}_t}{\sqrt{\alpha_t}},$$

where  $\alpha_t = \prod_{s=1}^t (1 - \beta_s)$  is the cumulative product of the noise schedule.

However, Lotus (He et al., 2024) shows that  $\epsilon$ -prediction injects unnecessary stochastic variation, which accumulates across multiple denoising steps, degrading dense prediction quality. Lotus therefore advocates a **deterministic** adaptation, directly predicting the clean annotation latent  $x_0$  in a single step:

$$\hat{x}_0 = g_\theta(z_T),$$

where  $T$  is a fixed timestep and  $g_\theta$  is fine-tuned U-Net applied once. This formulation eliminates the prediction variance introduced by multiple-step denoising, simplifies optimization, and significantly accelerates inference. In our approach, we similarly avoid the diffusion chain and adopt this  $x_0$ -prediction design.

### 4 METHODOLOGY

#### 4.1 LEVERAGING THE MULTI-SCALE LATENT FEATURES FOR POSE ESTIMATION

In this paper, we directly leverage the multi-scale latent features of SD U-Net for the pose estimation task. The input image is encoded by the frozen SD-VAE encoder and then fed into the SD U-Net, from which we extract multi-scale features at the upsampling stage. These features serve as robust representations for downstream applications. The choice of feature map depends on the keypoint granularity: for the 17-keypoint setting, we use the last-layer upsampling features, while for the 133-keypoint whole-body setting, we use the second-to-last upsampling features, as validated in Sec. 5.4.2.

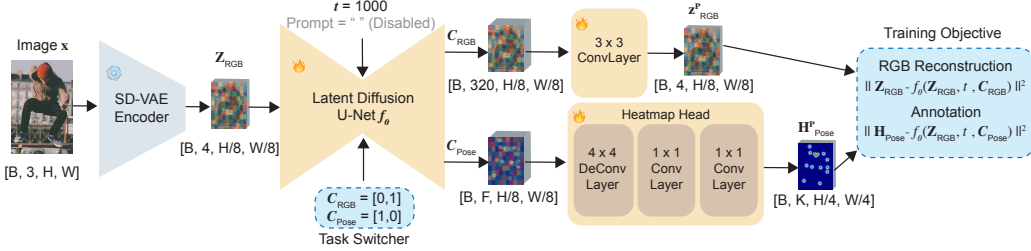


**Figure 2: Training Pipeline of SDPose.** The input RGB image is first encoded into the latent space by a pre-trained VAE. The U-Net is conditioned for multi-task learning via a class embedding. When the class label is set to [0,1], the U-Net predicts the reconstructed RGB latent; when set to [1,0], it produces features for heatmap prediction. The output layer of the U-Net is task-specific: the original convolutional output layer is retained for RGB latent reconstruction, while a lightweight heatmap decoder is used to process the U-Net’s intermediate features for keypoint heatmap prediction.

#### 4.2 THE U-NET CONVOLUTIONAL OUTPUT LAYER FORMS AN INFORMATION BOTTLENECK

Stable Diffusion’s U-Net outputs a 4-channel latent  $z \in \mathbb{R}^{4 \times h \times w}$  for the VAE through a single convolutional layer. In contrast, pose estimation requires  $K$ -channel heatmaps  $H \in \mathbb{R}^{K \times H' \times W'}$  with  $K \gg 4$ , making the 4-channel latent a severe information bottleneck. To address this, we replace the original 4-channel head with a lightweight heatmap decoder (Xiao et al., 2018). The decoder consists of a deconvolution layer for upsampling, followed by two  $1 \times 1$  convolutions that output  $K$ -channel heatmaps (Fig. 2). This modification removes the bottleneck and shortens the supervision path to keypoints.

#### 4.3 AUXILIARY RGB RECONSTRUCTION

To preserve the fine-detail representation capability of diffusion priors and to avoid overfitting to the pose estimation domain, we adopt the *Detail Preserver* strategy from Lotus (He et al., 2024). Concretely, we introduce a class embedding  $C \in \{C_{\text{RGB}}, C_{\text{Pose}}\}$  that controls the behavior of the denoising U-Net  $f_\theta$ . When  $C_{\text{RGB}}$  is provided, the network is trained to reconstruct the RGB latent  $z_{\text{RGB}}$ ; when  $C_{\text{Pose}}$  is provided, it learns to reconstruct the ground-truth heatmap  $H_{\text{Pose}}$ . The overall objective is

$$L = \|z_{\text{RGB}} - f_\theta(z_{\text{input}}, t, C_{\text{RGB}})\|^2 + \|H_{\text{Pose}} - f_\theta(z_{\text{input}}, t, C_{\text{Pose}})\|^2,$$

where  $z_{\text{input}}$  is the latent encoded from the input image by the SD-VAE, and  $t$  is fixed to  $t = 1000$  in our experiments.

#### 4.4 INFERENCE

As illustrated in Fig. 3, the input RGB image  $x$  is encoded by the SD-VAE into the latent representation  $z_{\text{RGB}}$ . The latent diffusion U-Net then performs a single-step regression with the timestep fixed at  $t = 1000$ , using the class label  $C_{\text{Pose}}$  to execute the pose estimation task. The text condition is disabled by feeding an empty text embedding to the U-Net.

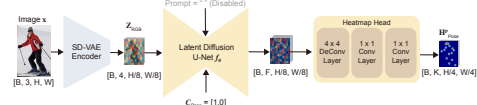


**Figure 3: SDPose Inference Pipeline.**

## 5 EXPERIMENTS

### 5.1 EXPERIMENT SETTINGS

**Implementation Details.** We train SDPose based on Stable Diffusion V2 (Rombach et al., 2022), with text conditioning disabled. During training, we fix the timestep  $t = 1000$ . For more details, please see the supplementary materials.

**Training Datasets.** We train two variants, SDPose 17-keypoints and SDPose 133-keypoints, on MS COCO (Lin et al., 2014) and COCO-WholeBody (Jin et al., 2020), respectively. All images are processed using standard top-down augmentations, with the input resolution set to  $1024 \times 768$ . Further details are provided in the supplementary materials.

**Validation Datasets and Metrics.** (1) For the 17-keypoint variant, we evaluate SDPose on MS COCO (Lin et al., 2014) for real-world images, and on HumanArt (Ju et al., 2023) and COCO-OOD for cross-domain benchmarks. (2) For the 133-keypoint variant, we evaluate SDPose on COCO-WholeBody (Jin et al., 2020) and the extended COCO-OOD. Further details of the evaluation datasets and metrics are provided in the supplementary materials.

**COCO-OOD (style-transferred COCO).** To complement HumanArt and enable OOD evaluation with matched content/labels, we translate all COCO val images into Monet-style paintings using the official CycleGAN framework (Zhu et al., 2017) (*monet2photo*), *preserving* the original human annotations (boxes, keypoints). This yields an OOD split with unchanged scene geometry but shifted texture, color, and brush patterns. The domain shift is further quantified by a Fréchet Inception Distance (FID) (Heusel et al., 2017) of 46.23 between COCO-OOD and the original COCO validation images, which is notably larger than the 32.59 FID measured between COCO validation and HumanArt.

Please refer to the supplementary materials for additional details.

### 5.2 QUANTITATIVE AND QUALITATIVE COMPARISON ON REAL-WORLD SCENES

Table 1: **Quantitative comparison on the COCO validation set.** We compare methods with parameter sizes comparable to the SDPose pipeline.

Model	Pre-trained Backbone	Parameters	Input size	Train dataset	Train epochs	AP	AR
Sapiens-1B (Khirodkar et al., 2024)	Sapiens ViT	1.169B	$1024 \times 768$	COCO	210	82.1	85.9
Sapiens-2B (Khirodkar et al., 2024)	Sapiens ViT	2.163B	$1024 \times 768$	COCO	210	<b>82.2</b>	<b>86.0</b>
GenLoc (Wang et al., 2025a)	Stable Diffusion-v1.5	0.95B	N/A	COCO	14	77.6	80.7
ViTPose ++-H (Xu et al., 2023)	ViTAE	0.63B	$256 \times 192$	Mixture*	210	79.4	N/A
SDPose (Ours)	Stable Diffusion-v1.5	0.95B	$1024 \times 768$	COCO	40	81.2	85.3
SDPose (Ours)	Stable Diffusion-v2	0.95B	$1024 \times 768$	COCO	40	81.3	85.2

\* Mixture includes COCO, AIC, MPII, AP10K, APT36K, and WholeBody datasets.

For the 17-keypoints variant, SDPose achieves 81.3 AP / 85.2 AR on the COCO validation set (Table 1) with only 40 training epochs using a 0.95B SD-v2 backbone. It matches the accuracy of Sapiens (82.1–82.2 AP) despite requiring 5× fewer epochs and a smaller backbone, and surpasses GenLoc (+3.7 AP, +4.5 AR). SDPose also outperforms ViTPose++ (+1.9 AP), which relies on multiple auxiliary datasets, while being trained solely on COCO. Figure 5 further illustrates robustness on real-world photos, where SDPose rivals Sapiens and corrects its failure cases (e.g., Sichuan opera eye keypoints). For the 133-keypoints variant, SDPose achieves competitive performance with Sapiens-1B on the COCO-WholeBody validation set. Further details are provided in the supplementary materials.

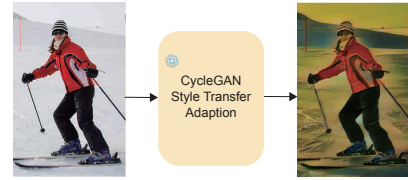


Figure 4: **COCO-OOD visualization.** COCO images are stylized into a Monet-like oil painting domain.

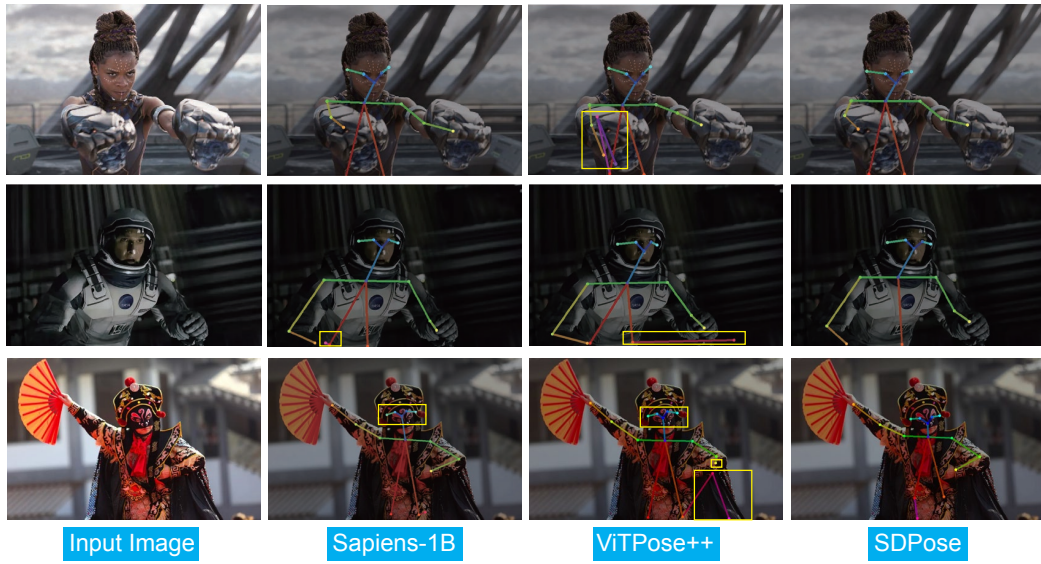


Figure 5: **Qualitative results on real-world photographs.** The yellow boxes highlight regions where baselines fail to predict accurate poses.

Table 2: **Quantitative comparison on OOD benchmarks HumanArt and COCO-OOD.** Here, we report the methods with parameter sizes comparable to the SDPose pipeline. All models are trained on COCO with an input size of  $1024 \times 768$ ; full HumanArt results for other methods are in the supplementary.

Model	Pre-trained Backbone	Parameters	Train epochs	HumanArt		COCO-OOD	
				AP	AR	AP	AR
Sapiens-1B (Khirodkar et al., 2024)	Sapiens ViT	1.169B	210	64.3	67.4	58.8	63.3
Sapiens-2B (Khirodkar et al., 2024)	Sapiens ViT	2.163B	210	69.6	72.2	59.6	64.0
GenLoc (Wang et al., 2025a)	Stable Diffusion-v1.5	0.95B	14	67.0	70.8	N/A	N/A
<b>SDPose (Ours)</b>	Stable Diffusion-v2	0.95B	40	<b>71.2</b>	<b>73.9</b>	<b>63.5</b>	<b>68.2</b>

### 5.3 SDPOSE'S STRONG OOD ROBUSTNESS

In this section, we demonstrate the superior OOD robustness of SDPose using quantitative evaluation on HumanArt and our COCO-OOD benchmark. As shown in Table 2, SDPose achieves state-of-the-art results on HumanArt and COCO-OOD with fewer training epochs and a smaller parameter budget. On COCO-OOD WholeBody (Table 3), SDPose continues to demonstrate strong out-of-domain robustness. As shown in Fig. 1, SDPose achieves more accurate body pose estimation across diverse animation styles and humanoid robots compared with baseline models. Additional qualitative results on whole-body pose estimation in stylized paintings are provided in the supplementary materials.

Table 3: **Quantitative comparison on the COCO-OOD Wholebody validation set.** In this section, we report only the whole-body AP and AR; please refer to the supplementary materials for detailed results on individual body parts.

Model	Pre-trained Backbone	Parameters	Input size	Train dataset	Train epochs	Whole AP	Whole AR
Sapiens-1B (Khirodkar et al., 2024)	Sapiens ViT	1.169B	$1024 \times 768$	COCO	210	38.7	46.8
Sapiens-2B (Khirodkar et al., 2024)	Sapiens ViT	2.163B	$1024 \times 768$	COCO	210	44.4	53.0
<b>SDPose (Ours)</b>	Stable Diffusion-v2	0.95B	$1024 \times 768$	COCO	42	<b>46.6</b>	<b>54.8</b>

## 5.4 ABLATION STUDY

### 5.4.1 ABLATION ON AUXILIARY RECONSTRUCTION TASK AND DIFFUSION PRIORS

We conduct ablations to validate our designs. For the “w/o diffusion priors” variant, we train the U-Net from scratch (no pretrained priors). For the “w/o RGB recon.” variant, we disable only the auxiliary RGB reconstruction branch; all other settings remain identical. From Table 4, two trends emerge. First, removing the RGB branch yields a consistent but modest AP/AR drop on COCO that becomes more pronounced on HumanArt and COCO-OOD, indicating that the auxiliary reconstruction acts as a useful regularizer and improves robustness under domain shift. Second, removing diffusion priors causes a much larger degradation, especially on the OOD benchmarks, highlighting that the pretrained generative priors are the primary source of SDPose’s generalization.

**Table 4: Ablation studies on the diffusion priors and RGB reconstruction branch.**  
All experiments are trained on COCO 17-keypoints with input  $1024 \times 768$  for 40 epochs.

Method	COCO		HumanArt		COCO-OOD	
	AP	AR	AP	AR	AP	AR
SDPose	81.3	85.2	71.2	73.9	63.5	68.2
SDPose w/o RGB Recon.	80.8 (-0.5)	84.9 (-0.3)	69.8 (-1.4)	72.6 (-1.3)	62.5 (-1.0)	67.3 (-0.9)
SDPose w/o Diffusion Priors	74.9 (-6.4)	79.4 (-5.8)	53.8 (-17.4)	58.0 (-15.9)	52.7 (-10.8)	57.9 (-10.3)

### 5.4.2 ABLATION ON MULTI-SCALE FEATURES FROM THE SD U-NET

Prior work ([Liu et al., 2023b; 2024; 2023a](#); [Wang et al., 2025b](#)) suggests that penultimate features often transfer better than final ones. As shown in Table 5, SDPose-17 favors the last-layer feature, while SDPose-133 benefits from the second-to-last. This indicates that the optimal feature choice depends on keypoint granularity: coarse 17-keypoint settings are well served by the final representation, whereas whole-body localization gains from the richer semantics in the penultimate layer.

**Table 5: Ablation on U-Net feature selection for the pose head.** All models are trained on COCO (40 epochs for 17-keypoints, 42 epochs for 133-keypoints).

Feature	SDPose-17		SDPose-133	
	AP	AR	AP	AR
Last layer	81.3	85.2	70.5	77.5
Second-to-last layer	81.1	85.0	71.5	78.4

## 6 ZERO-SHOT DOWNSTREAM APPLICATIONS

### 6.1 BETTER POSE-GUIDED IMAGE GENERATION

For human or humanoid character generation, an accurate skeleton is essential for transferring poses between characters. Traditional pose estimators often fail to precisely capture the skeletons of art-based human or humanoid characters. Our method provides a generalizable pose estimation approach that can benefit animation production. As shown in Fig. 6, we compare ControlNet ([Zhang et al., 2023](#)) outputs using DWPose as the baseline pose annotator. Notably, our SDPose yields more precise and detailed skeletons than DWPose, enabling reliable pose transfer and high-quality image generation for artistic characters.

### 6.2 POSE-GUIDED VIDEO GENERATION

Recent advances in controlled video generation have gained significant traction ([Hu, 2024](#); [Guo et al., 2023](#); [Kim et al., 2024](#)). Despite the progress of video generation models in producing higher-quality outputs, extracting reliable control conditions remains critical for achieving high-quality results. As shown in Fig. 7, our SDPose provides more accurate

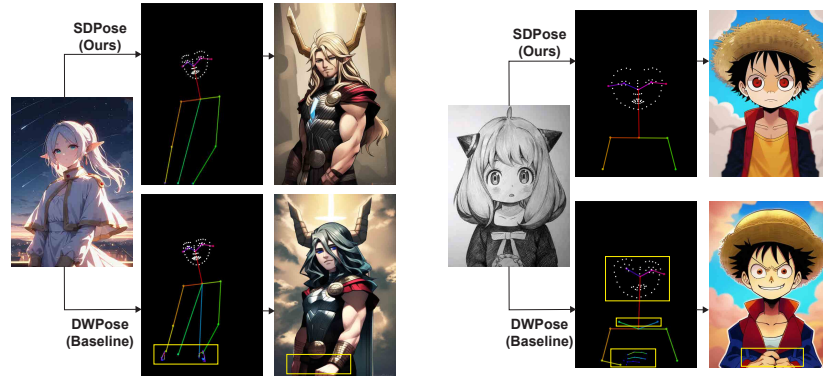


Figure 6: **Visualization of pose-guided image generation results.** The lower images illustrate results from the baseline, which combines a pre-trained ControlNet with the DW-Pose estimator. In comparison, the upper images show results obtained using our SDPose as the pose annotator. Yellow boxes highlight baseline failures. Prompts, random seeds, and other settings are kept identical for fairness.

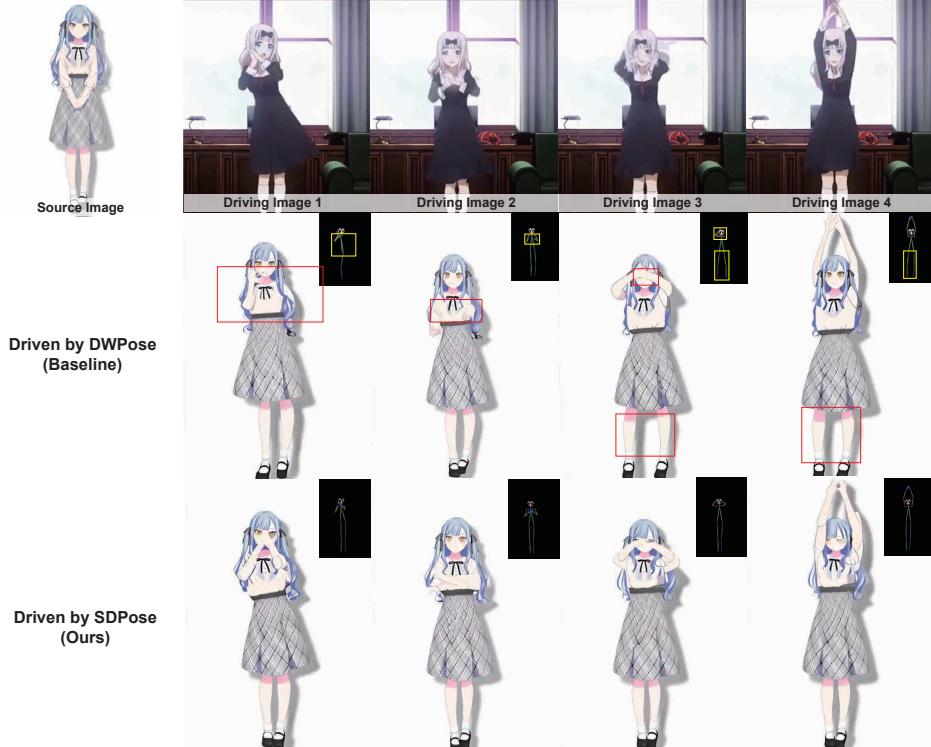


Figure 7: **Qualitative comparison for pose-controlled video generation in the wild.** The first row shows the source image and frames from the driving video. The second row shows output video frames generated from the pose sequence estimated by the baseline model DWPose, while the third row shows the results guided by our SDPose. Red boxes highlight failures in the generated video, and yellow boxes highlight errors in pose estimation.

poses for the driving frames, enabling more reliable pose-sequence transfer from animations to animations. Video frames are generated by Moore-Animated Anyone<sup>1</sup>.

<sup>1</sup><https://github.com/MooreThreads/Moore-AnimateAnyone>

## 7 CONCLUSION

In this paper, we present **SDPose**, an SD-native fine-tuning strategy for human pose estimation. SDPose preserves the original U-Net with only lightweight task-specific components, adapting generative latent priors for keypoint prediction through an auxiliary RGB reconstruction branch and a heatmap decoder. We further introduce **COCO-OOD**, a style-transferred extension of COCO for evaluating robustness under domain shifts. With only 1/5 of Sapiens' fine-tuning cost and a smaller backbone, SDPose matches its accuracy on COCO and achieves state-of-the-art results on COCO-OOD and HumanArt, demonstrating strong generalization for pose estimation.

### ETHICS STATEMENT

This work builds upon publicly available datasets (COCO, COCO Wholebody), all of which have established licenses and annotation protocols. No private or personally identifiable information is used. Our method focuses on improving the robustness of pose estimation under domain shifts, which can benefit applications such as animation and embodied AI.

### REPRODUCIBILITY STATEMENT

We have made every effort to ensure reproducibility. All datasets used are publicly available, and we detail dataset splits, preprocessing steps, and evaluation protocols in Sec. 4. Our training settings, hyperparameters, and model architectures are fully described in Sec. 4, Sec. 5 and Appendix A. Code and scripts to reproduce our experiments will be released upon publication.

### REFERENCES

- Xiangqi Chen, Chengzhan Yang, Jiashuaizi Mo, Yixin Sun, Hicham Karmouni, Yunliang Jiang, and Zhonglong Zheng. Cspnext: A new efficient token hybrid backbone. *Engineering Applications of Artificial Intelligence*, 132:107886, 2024.
- Yen-Chi Cheng, Hsin-Ying Lee, Sergey Tulyakov, Alexander G Schwing, and Liang-Yan Gui. Sdfusion: Multimodal 3d shape completion, reconstruction, and generation. In *Proceedings of the IEEE/CVF conference on computer vision and pattern recognition*, pp. 4456–4465, 2023.
- Patrick Esser, Sumith Kulal, Andreas Blattmann, Rahim Entezari, Jonas Müller, Harry Saini, Yam Levi, Dominik Lorenz, Axel Sauer, Frederic Boesel, et al. Scaling rectified flow transformers for high-resolution image synthesis. In *Forty-first international conference on machine learning*, 2024.
- Yuwei Guo, Ceyuan Yang, Anyi Rao, Zhengyang Liang, Yaohui Wang, Yu Qiao, Maneesh Agrawala, Dahua Lin, and Bo Dai. Animatediff: Animate your personalized text-to-image diffusion models without specific tuning. *arXiv preprint arXiv:2307.04725*, 2023.
- Jing He, Haodong Li, Wei Yin, Yixun Liang, Leheng Li, Kaiqiang Zhou, Hongbo Liu, Bingbing Liu, and Ying-Cong Chen. Lotus: Diffusion-based visual foundation model for high-quality dense prediction. *arXiv preprint arXiv:2409.18124*, 2024.
- Martin Heusel, Hubert Ramsauer, Thomas Unterthiner, Bernhard Nessler, and Sepp Hochreiter. Gans trained by a two time-scale update rule converge to a local nash equilibrium. *Advances in neural information processing systems*, 30, 2017.
- Jonathan Ho, Ajay Jain, and Pieter Abbeel. Denoising diffusion probabilistic models. *Advances in neural information processing systems*, 33:6840–6851, 2020.
- Li Hu. Animate anyone: Consistent and controllable image-to-video synthesis for character animation. In *Proceedings of the IEEE/CVF Conference on Computer Vision and Pattern Recognition*, pp. 8153–8163, 2024.

- Junjie Huang, Zheng Zhu, Feng Guo, and Guan Huang. The devil is in the details: Delving into unbiased data processing for human pose estimation. In *Proceedings of the IEEE/CVF conference on computer vision and pattern recognition*, pp. 5700–5709, 2020.
- Tao Jiang, Peng Lu, Li Zhang, Ningsheng Ma, Rui Han, Chengqi Lyu, Yining Li, and Kai Chen. Rtmpose: Real-time multi-person pose estimation based on mmpose. *arXiv preprint arXiv:2303.07399*, 2023.
- Sheng Jin, Lumin Xu, Jin Xu, Can Wang, Wentao Liu, Chen Qian, Wanli Ouyang, and Ping Luo. Whole-body human pose estimation in the wild. In *Proceedings of the European Conference on Computer Vision (ECCV)*, 2020.
- Xuan Ju, Ailing Zeng, Jianan Wang, Qiang Xu, and Lei Zhang. Human-art: A versatile human-centric dataset bridging natural and artificial scenes. In *Proceedings of the IEEE/CVF Conference on Computer Vision and Pattern Recognition*, 2023.
- Markus Karmann and Onay Urfalioglu. Repurposing stable diffusion attention for training-free unsupervised interactive segmentation. In *Proceedings of the Computer Vision and Pattern Recognition Conference*, pp. 24518–24528, 2025.
- Bingxin Ke, Anton Obukhov, Shengyu Huang, Nando Metzger, Rodrigo Caye Daudt, and Konrad Schindler. Repurposing diffusion-based image generators for monocular depth estimation. In *Proceedings of the IEEE/CVF conference on computer vision and pattern recognition*, pp. 9492–9502, 2024.
- Rawal Khirodkar, Timur Bagautdinov, Julieta Martinez, Su Zhaoen, Austin James, Peter Selednik, Stuart Anderson, and Shunsuke Saito. Sapiens: Foundation for human vision models. In *European Conference on Computer Vision*, pp. 206–228. Springer, 2024.
- Jeongho Kim, Min-Jung Kim, Junsoo Lee, and Jaegul Choo. Tcan: Animating human images with temporally consistent pose guidance using diffusion models. In *European Conference on Computer Vision*, pp. 326–342. Springer, 2024.
- Jiantao Lin, Xin Yang, Meixi Chen, Yingjie Xu, Dongyu Yan, Leyi Wu, Xinli Xu, Lie Xu, Shunsi Zhang, and Ying-Cong Chen. Kiss3dgen: Repurposing image diffusion models for 3d asset generation. In *Proceedings of the Computer Vision and Pattern Recognition Conference*, pp. 5870–5880, 2025.
- Tsung-Yi Lin, Michael Maire, Serge Belongie, James Hays, Pietro Perona, Deva Ramanan, Piotr Dollár, and C Lawrence Zitnick. Microsoft coco: Common objects in context. In *European conference on computer vision*, pp. 740–755. Springer, 2014.
- Yaron Lipman, Ricky TQ Chen, Heli Ben-Hamu, Maximilian Nickel, and Matt Le. Flow matching for generative modeling. *arXiv preprint arXiv:2210.02747*, 2022.
- Haotian Liu, Chunyuan Li, Yuheng Li, and Yong Jae Lee. Improved baselines with visual instruction tuning, 2023a.
- Haotian Liu, Chunyuan Li, Qingyang Wu, and Yong Jae Lee. Visual instruction tuning, 2023b.
- Haotian Liu, Chunyuan Li, Yuheng Li, Bo Li, Yuanhan Zhang, Sheng Shen, and Yong Jae Lee. Llava-next: Improved reasoning, ocr, and world knowledge, January 2024. URL <https://llava-v1.github.io/blog/2024-01-30-llava-next/>.
- Xiaoxiao Long, Yuan-Chen Guo, Cheng Lin, Yuan Liu, Zhiyang Dou, Lingjie Liu, Yuexin Ma, Song-Hai Zhang, Marc Habermann, Christian Theobalt, et al. Wonder3d: Single image to 3d using cross-domain diffusion. In *Proceedings of the IEEE/CVF conference on computer vision and pattern recognition*, pp. 9970–9980, 2024.
- Cheng Lu, Yuhao Zhou, Fan Bao, Jianfei Chen, Chongxuan Li, and Jun Zhu. Dpm-solver: A fast ode solver for diffusion probabilistic model sampling in around 10 steps. *Advances in neural information processing systems*, 35:5775–5787, 2022.

- Ginés Hidalgo Martínez. *Openpose: Whole-body pose estimation*. PhD thesis, Carnegie Mellon University Pittsburgh, PA, USA, 2019.
- William Peebles and Saining Xie. Scalable diffusion models with transformers. In *Proceedings of the IEEE/CVF international conference on computer vision*, pp. 4195–4205, 2023.
- Robin Rombach, Andreas Blattmann, Dominik Lorenz, Patrick Esser, and Björn Ommer. High-resolution image synthesis with latent diffusion models. In *Proceedings of the IEEE/CVF conference on computer vision and pattern recognition*, pp. 10684–10695, 2022.
- Christoph Schuhmann, Romain Beaumont, Richard Vencu, Cade Gordon, Ross Wightman, Mehdi Cherti, Theo Coombes, Aarush Katta, Clayton Mullis, Mitchell Wortsman, et al. Laion-5b: An open large-scale dataset for training next generation image-text models. *Advances in neural information processing systems*, 35:25278–25294, 2022.
- Jiaming Song, Chenlin Meng, and Stefano Ermon. Denoising diffusion implicit models. *arXiv preprint arXiv:2010.02502*, 2020a.
- Yang Song, Jascha Sohl-Dickstein, Diederik P Kingma, Abhishek Kumar, Stefano Ermon, and Ben Poole. Score-based generative modeling through stochastic differential equations. *arXiv preprint arXiv:2011.13456*, 2020b.
- Ke Sun, Bin Xiao, Dong Liu, and Jingdong Wang. Deep high-resolution representation learning for human pose estimation. In *Proceedings of the IEEE/CVF conference on computer vision and pattern recognition*, pp. 5693–5703, 2019.
- Ke Sun, Zigang Geng, Depu Meng, Bin Xiao, Dong Liu, Zhaoxiang Zhang, and Jingdong Wang. Bottom-up human pose estimation by ranking heatmap-guided adaptive keypoint estimates. *arXiv preprint arXiv:2006.15480*, 2020.
- Dongkai Wang, Jiang Duan, Liangjian Wen, Shiyu Xuan, Hao Chen, and Shiliang Zhang. Generalizable object keypoint localization from generative priors. In *Proceedings of the Computer Vision and Pattern Recognition Conference*, pp. 20265–20274, 2025a.
- Zeqing Wang, Qingyang Ma, Wentao Wan, Haojie Li, Keze Wang, and Yonghong Tian. Is this generated person existed in real-world? fine-grained detecting and calibrating abnormal human-body. In *Proceedings of the Computer Vision and Pattern Recognition Conference*, pp. 21226–21237, 2025b.
- Bin Xiao, Haiping Wu, and Yichen Wei. Simple baselines for human pose estimation and tracking. In *Proceedings of the European conference on computer vision (ECCV)*, pp. 466–481, 2018.
- Enze Xie, Junsong Chen, Junyu Chen, Han Cai, Haotian Tang, Yujun Lin, Zhekai Zhang, Muyang Li, Ligeng Zhu, Yao Lu, et al. Sana: Efficient high-resolution image synthesis with linear diffusion transformers. *arXiv preprint arXiv:2410.10629*, 2024.
- Guangkai Xu, Yongtao Ge, Mingyu Liu, Chengxiang Fan, Kangyang Xie, Zhiyue Zhao, Hao Chen, and Chunhua Shen. What matters when repurposing diffusion models for general dense perception tasks? *arXiv preprint arXiv:2403.06090*, 2024.
- Yufei Xu, Jing Zhang, Qiming Zhang, and Dacheng Tao. Vitpose: Simple vision transformer baselines for human pose estimation. *Advances in neural information processing systems*, 35:38571–38584, 2022.
- Yufei Xu, Jing Zhang, Qiming Zhang, and Dacheng Tao. Vitpose++: Vision transformer for generic body pose estimation. *IEEE Transactions on Pattern Analysis and Machine Intelligence*, 46(2):1212–1230, 2023.
- Zhendong Yang, Ailing Zeng, Chun Yuan, and Yu Li. Effective whole-body pose estimation with two-stages distillation. In *Proceedings of the IEEE/CVF International Conference on Computer Vision*, pp. 4210–4220, 2023.

Yuhui Yuan, Rao Fu, Lang Huang, Weihong Lin, Chao Zhang, Xilin Chen, and Jingdong Wang. Hrformer: High-resolution transformer for dense prediction. 2021.

Lvmin Zhang, Anyi Rao, and Maneesh Agrawala. Adding conditional control to text-to-image diffusion models. In *Proceedings of the IEEE/CVF International Conference on Computer Vision*, pp. 3836–3847, 2023.

Zhengbo Zhang, Li Xu, Duo Peng, Hossein Rahmani, and Jun Liu. Diff-tracker: text-to-image diffusion models are unsupervised trackers. In *European Conference on Computer Vision*, pp. 319–337. Springer, 2024.

Jun-Yan Zhu, Taesung Park, Phillip Isola, and Alexei A Efros. Unpaired image-to-image translation using cycle-consistent adversarial networkss. In *Computer Vision (ICCV), 2017 IEEE International Conference on*, 2017.

## SUPPLEMENTARY MATERIALS FOR SDPOSE: EXPLOITING DIFFUSION PRIORS FOR OUT-OF-DOMAIN AND ROBUST POSE ESTIMATION

### A EXPERIMENT SETTINGS

#### A.1 IMPLEMENTATION DETAILS

We train SDPose on the COCO-2017 person keypoints *train2017* split only (no extra data), with text prompts disabled. The diffusion timestep is fixed at  $t = 1000$ . We use AdamW with a learning rate of  $3 \times 10^{-5}$ . All experiments are run on 8 NVIDIA A100-NVLink GPUs with a total batch size of 128, without gradient accumulation. Inputs are resized to  $1024 \times 768$  with standard top-down augmentations. The 17-keypoint model is trained for 40 epochs (approximately 3 days), and the 133-keypoint model for 42 epochs (approximately 3 days and a half).

#### A.2 TRAINING DATASETS

**COCO 2017 Keypoint Detection** We train the 17-keypoint variant on the COCO-2017 person keypoint detection dataset (Lin et al., 2014). The full COCO release contains more than 200,000 images and about 250,000 person instances. Person keypoint annotations follow the 17-point format (nose, eyes, ears, shoulders, elbows, wrists, hips, knees, and ankles).

**COCO Wholebody** To further evaluate large-scale whole-body keypoint estimation, we adopt COCO-WholeBody (Jin et al., 2020), an extended benchmark built on top of COCO images. COCO-WholeBody augments the original 17 body joints with fine-grained annotations of foot (6 keypoints), face (68 keypoints), and hands (42 keypoints for hands), resulting in a total of 133 keypoints per person. The dataset provides consistent whole-body annotations across the same training and validation splits as COCO-2017, enabling both fair comparison with standard pose estimation methods and comprehensive evaluation under the whole-body setting.

#### A.3 AUGMENTATION DETAILS

The training pipeline first loads the input image and computes the bounding box center and scale. It applies random horizontal flipping, half-body augmentation, and random bounding box transformations. The image is then affine-transformed to the target input resolution using UDP (Huang et al., 2020). Albumentations-based augmentations are then applied, including Gaussian blur ( $p = 0.1$ ), median blur ( $p = 0.1$ ), and coarse dropout ( $p = 1.0$ , with up to one hole of size 20%–40% of the image).

#### A.4 EVALUATION DATASETS AND METRICS

##### Evaluation Datasets

**COCO 2017 Keypoint Detection.** For in-domain evaluation, we use the COCO-2017 validation set (Lin et al., 2014) annotated with 17 body keypoints, bounding boxes, and visibility flags. Following the standard top-down evaluation protocol, we generate person crops from the COCO-released detection results (`COCO_val2017_detections_AP_H_70_person.json`), and report COCO keypoint AP/AR on this diverse in-the-wild dataset.

**HumanArt.** We use HumanArt (Ju et al., 2023) as an cross domain benchmark: 50k human-centric images across 20 scenarios (5 natural, 15 artistic—oil painting, sculpture, cartoon, sketch, stained glass, Ukiyo-e, watercolor, etc.) with annotations for boxes and 2D keypoints. We follow the official protocol and report keypoint AP/AR to assess robustness under artistic domain shift.

**COCO-WholeBody (133-keypoint whole-body).** We train and evaluate a 133-keypoint variant on COCO-WholeBody (Jin et al., 2020), which shares COCO’s

train/val split. Each person has 133 keypoints (17 body, 6 foot, 68 face, 42 hand) plus boxes for person/face/left/right hand. We follow the official protocol and report Whole-Body AP and part-wise AP (body/foot/face/hand). This dataset spans diverse in-the-wild scenes and stresses fine-grained articulation, complementing COCO for structured keypoint evaluation.

**Metrics** We follow the standard COCO keypoint evaluation protocol, which is based on the Object Keypoint Similarity (OKS). For each keypoint  $i$ , the similarity is defined as

$$KS_i = \exp\left(-\frac{d_i^2}{2s^2k_i^2}\right),$$

where  $d_i$  denotes the Euclidean distance between predicted and ground-truth keypoints,  $s$  is the object scale (square root of the segmentation area), and  $k_i$  is a per-keypoint constant controlling falloff. The OKS for an instance is the average  $KS_i$  over visible keypoints:

$$OKS = \frac{\sum_i KS_i \cdot \delta(v_i > 0)}{\sum_i \delta(v_i > 0)},$$

where  $v_i$  is the visibility flag. Using OKS as the matching criterion, COCO computes Average Precision (AP) as the mean precision over OKS thresholds [0.50 : 0.05 : 0.95], and Average Recall (AR) analogously as the mean recall across the same thresholds.

## A.5 DETAILS OF COCO-OOD



Figure 8: **COCO-OOD visualizations with Monet-style oil painting.** We use CycleGAN to stylize COCO validation images into a Monet-like oil painting domain, creating an OOD split to evaluate pose estimation robustness under appearance shift.

To complement the HumanArt dataset and enable OOD evaluation under matched content and labels, we construct COCO-OOD by applying artistic style transfer to the original COCO images. We adopt the official CycleGAN framework (Zhu et al., 2017) to perform unpaired image-to-image translation from the COCO domain (natural photographs) to the target domain of Monet-style paintings. We use the `monet2photo` model provided in the CycleGAN repository, which is trained in an unsupervised manner to learn the mapping between Monet paintings and real-world photos. During conversion, all training and validation images in COCO are processed to produce style-transferred counterparts, while preserving their original human annotations (bounding boxes, keypoints). This yields an OOD variant of COCO in which the underlying scene structure is unchanged, but the texture, color palette, and brushstroke patterns are consistent with Monet’s artistic style. Importantly, for

fair comparison and to avoid introducing priors from large-scale pretrained diffusion models, we intentionally adopt the earlier CycleGAN framework rather than more recent style transfer methods. Such stylization introduces a significant appearance shift while keeping pose-related geometric information intact, making it suitable for robust pose estimation evaluation.

## B DETAILS OF QUANTITATIVE COMPARISON AND ADDITIONAL QUALITATIVE COMPARISON

### B.1 FULL QUANTITATIVE COMPARISON ON COCO

Table 6: Quantitative comparison on the COCO validation set.

Model	Input Size	AP	AR
SimpleBaseline (Xiao et al., 2018)	256×192	73.5	79.0
HRNet (Sun et al., 2019)	384×288	76.3	81.2
HRFormer (Yuan et al., 2021)	256×192	77.2	82.0
ViTPose-S (Xu et al., 2022)	256×192	73.8	79.2
ViTPose-B (Xu et al., 2022)	256×192	75.8	81.1
ViTPose-L (Xu et al., 2022)	256×192	78.3	83.5
ViTPose-H (Xu et al., 2022)	256×192	79.1	84.1
ViTPose++-S (Xu et al., 2023)	256×192	75.8	81.0
ViTPose++-B (Xu et al., 2023)	256×192	77.0	82.6
ViTPose++-L (Xu et al., 2023)	256×192	78.6	84.1
ViTPose++-H (Xu et al., 2023)	256×192	79.4	84.8
Sapiens-0.3B (Khirodkar et al., 2024)	1024×768	79.6	83.6
Sapiens-0.6B (Khirodkar et al., 2024)	1024×768	81.2	84.9
Sapiens-1B (Khirodkar et al., 2024)	1024×768	82.1	85.9
Sapiens-2B (Khirodkar et al., 2024)	1024×768	82.2	86.0
<b>SDPose (Ours)</b>	1024×768	<b>81.3</b>	<b>85.2</b>

### B.2 FULL QUANTITATIVE COMPARISON ON HUMANART

On HumanArt (Table 7), SDPose sets a new state of the art with 71.2 AP / 73.9 AR, surpassing large-scale foundation baselines under the same COCO-only training: +1.6 AP over Sapiens-2B (69.6 AP) and +4.7 AP over ViTPose-H (66.5 AP), with consistent AR gains. Compared with traditional baselines such as RTMPose (Jiang et al., 2023) and HRNet (Sun et al., 2019), SDPose further delivers substantial improvements in AP, exceeding them by more than 14 points.

### B.3 FULL QUANTITATIVE COMPARISON ON COCO WHOLEBODY

As shown in Table 8, SDPose achieves 71.5 AP / 78.4 AR on the COCO-WholeBody validation set. This result is highly competitive with the large-scale Sapiens (Khirodkar et al., 2024) models: while Sapiens-2B reaches 74.4 AP with over 2B parameters and long training schedules, SDPose attains comparable accuracy with a smaller 0.95B backbone trained for only 42 epochs. In terms of sub-part analysis, our method closely matches Sapiens-2B on body (77.9 vs. 79.2) and feet (81.5 vs. 84.1), while maintaining strong performance on face (88.5 vs. 91.2). The largest gap appears on hand keypoints (65.2 vs. 70.4), reflecting the intrinsic difficulty of fine-grained articulation. Nevertheless, compared with classical baselines such as HRNet (Sun et al., 2019), RTMPose (Jiang et al., 2023), or DWPOse (Yang et al., 2023), SDPose shows substantial gains of +6–12 AP across whole-body evaluation.

Table 7: **Quantitative Comparison on the HumanArt validation set.** Models trained on COCO, evaluated with GT bounding boxes. SDPose achieves new state-of-the-art performance.

Model	AP	AP <sup>50</sup>	AP <sup>75</sup>	AR	AR <sup>50</sup>
RTMPose-T (Jiang et al., 2023)	44.4	72.5	45.3	48.8	75.0
RTMPose-S (Jiang et al., 2023)	48.0	73.9	49.8	52.1	76.3
RTMPose-M (Jiang et al., 2023)	53.2	76.5	56.3	57.1	78.9
RTMPose-L (Jiang et al., 2023)	56.4	78.9	60.2	59.9	80.8
ViTPose-S (Xu et al., 2022)	50.7	75.8	53.1	55.1	78.0
ViTPose-B (Xu et al., 2022)	55.5	78.2	59.0	59.9	80.9
ViTPose-L (Xu et al., 2022)	63.7	83.8	68.9	67.7	85.9
ViTPose-H (Xu et al., 2022)	66.5	86.0	71.5	70.1	87.1
HRNet-W32 (Sun et al., 2019)	53.3	77.1	56.2	57.4	79.2
HRNet-W48 (Sun et al., 2019)	55.7	78.2	59.3	59.5	80.4
Sapiens-1B (Khirodkar et al., 2024)	64.3	82.1	67.9	67.4	83.7
Sapiens-2B (Khirodkar et al., 2024)	69.6	85.3	73.3	72.2	86.8
<b>SDPose (Ours)</b>	<b>71.2</b>	<b>87.3</b>	<b>76.3</b>	<b>73.9</b>	<b>88.6</b>

Table 8: **Quantitative comparison on the COCO-WholeBody validation set.**

(a) Body, Feet, Face						
Model	Body AP	Body AR	Feet AP	Feet AR	Face AP	Face AR
HRNet (Sun et al., 2019)	70.1	77.3	58.6	69.2	72.7	78.3
VitPose+-L (Xu et al., 2023)	75.3	-	77.1	-	63.0	-
VitPose+-H (Xu et al., 2023)	75.9	-	77.9	-	63.6	-
RTMPose-x (Jiang et al., 2023)	71.4	78.4	69.2	81.0	88.8	92.2
DWPose-l (Yang et al., 2023)	72.2	78.9	70.4	81.7	88.7	92.1
Sapiens-0.3B (Khirodkar et al., 2024)	66.4	73.4	67.3	78.4	87.1	91.2
Sapiens-0.6B (Khirodkar et al., 2024)	74.3	80.2	79.4	87.0	89.5	92.9
Sapiens-1B (Khirodkar et al., 2024)	77.4	82.9	83.0	89.8	90.7	93.6
Sapiens-2B (Khirodkar et al., 2024)	<b>79.2</b>	<b>84.6</b>	<b>84.1</b>	<b>90.9</b>	<b>91.2</b>	<b>93.8</b>
SDPose (Ours)	77.9	83.4	81.5	88.7	88.5	92.2

(b) Hands and Whole-body				
Model	Hand AP	Hand AR	Whole AP	Whole AR
HRNet (Sun et al., 2019)	51.6	60.4	58.6	67.4
VitPose+-L (Xu et al., 2023)	54.2	-	60.6	-
VitPose+-H (Xu et al., 2023)	54.7	-	61.2	-
RTMPose-x (Jiang et al., 2023)	59.0	68.5	65.3	73.3
DWPose-l (Yang et al., 2023)	62.1	71.0	66.5	74.3
Sapiens-0.3B (Khirodkar et al., 2024)	58.1	67.1	62.0	69.4
Sapiens-0.6B (Khirodkar et al., 2024)	65.4	74.0	69.5	76.3
Sapiens-1B (Khirodkar et al., 2024)	69.2	77.1	72.7	79.2
Sapiens-2B (Khirodkar et al., 2024)	<b>70.4</b>	<b>78.1</b>	<b>74.4</b>	<b>81.0</b>
SDPose (Ours)	65.2	74.0	71.5	78.4

#### B.4 FULL QUANTITATIVE COMPARISON ON COCO-OOD WHOLEBODY

Detailed whole-body pose estimation results on COCO-OOD are reported in Table 9. Breaking down by body part, SDPose matches or surpasses Sapiens on the most stable regions: body (60.0 AP vs. 59.9) and feet (62.5 vs. 63.8), and delivers a notable margin on face landmarks (+5.8 AP, 64.2 vs. 58.4), highlighting the reliability of SD-native features under appearance shifts. For hands, which are the most challenging due to fine-grained articulation and limited resolution, SDPose attains 46.3/44.9 AP on left/right hands, respectively, remaining competitive but still slightly behind Sapiens-2B (48.2/46.8). Nevertheless, the

Table 9: **Quantitative Comparison on the COCO-OOD Wholebody validation set.**

(a) Body, Feet, Face						
Model	Body AP	Body AR	Feet AP	Feet AR	Face AP	Face AR
Sapiens-1B	52.1	58.6	55.9	66.2	57.6	63.0
Sapiens-2B	59.9	65.8	63.8	72.4	58.4	64.2
SDPose (Ours)	<b>60.0</b>	<b>66.1</b>	<b>62.5</b>	<b>72.0</b>	<b>64.2</b>	<b>69.9</b>

(b) Hands and Whole-body						
Model	L-Hand AP	L-Hand AR	R-Hand AP	R-Hand AR	Whole AP	Whole AR
Sapiens-1B	43.1	52.0	41.5	50.6	38.7	46.8
Sapiens-2B	48.2	56.8	46.8	55.3	44.4	53.0
SDPose (Ours)	46.3	55.2	44.9	54.4	<b>46.6</b>	<b>54.8</b>

overall whole-body AP/AR of 46.6/54.8 establishes SDPose as the most robust framework under OOD whole-body evaluation.

### B.5 QUALITATIVE COMPARISON FOR WHOLE-BODY POSE ESTIMATION

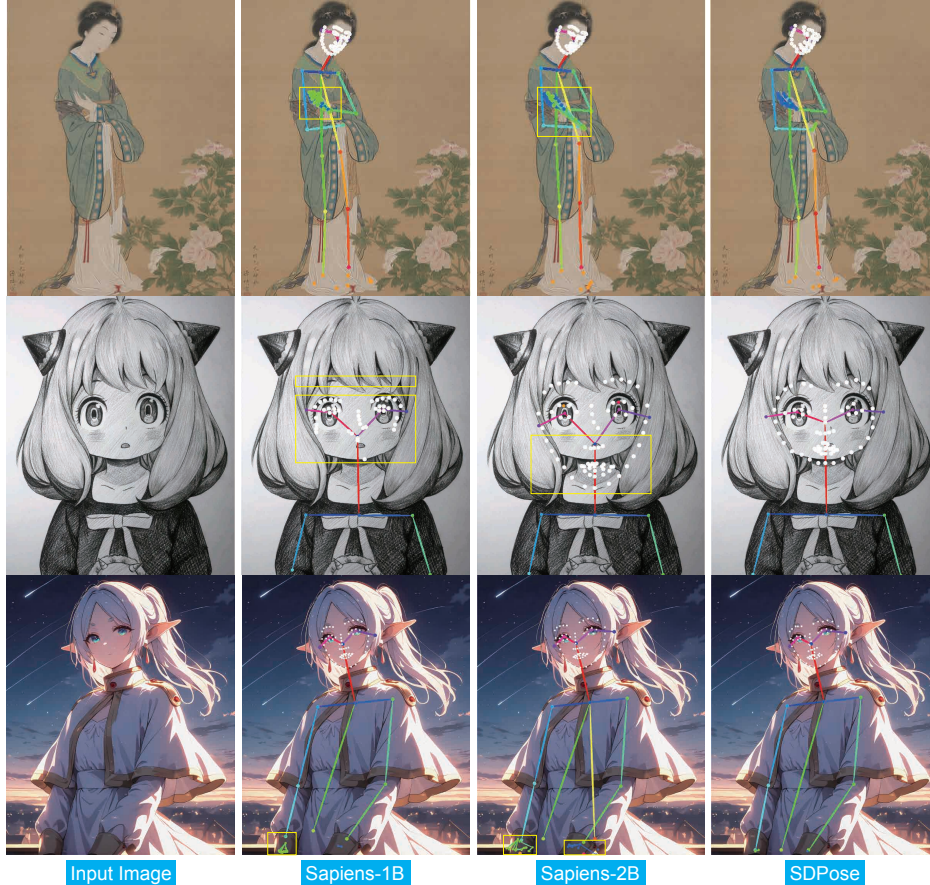


Figure 9: **Comparison on Stylized Paintings: Sapiens WholeBody vs. SDPose WholeBody.** All erroneous predictions are highlighted with yellow boxes. SDPose yields fewer false positives and notably better facial keypoint localization.